Available online at www.sciencedirect.com
ScienceDirect
Trans. Nonferrous Met. Soc. China 34(2024) 1263−1274
Transactions of Nonferrous Metals Society of China
www.tnmsc.cn

Occurrence state and distribution characteristics of tungsten in Dabaoshan tungsten-bearing goethite

Hong-hu TANG[1,2], Bing-jian LIU[1,2], Cui WANG[1,2], Xiong-xing ZHANG[1,2], Hai-sheng HAN[1,2], Li WANG[1,2], Yang CAO[1,2], Wei SUN[1,2]

1. School of Minerals Processing and Bioengineering, Central South University, Changsha 410083, China;
2. Hunan International Joint Research Center for Efficient and Clean Utilization of Critical Metal Mineral Resources, Central South University, Changsha 410083, China

Received 7 December 2022; accepted 7 June 2023

Abstract: The phase composition and elemental distribution of the tungsten-bearing goethite in Dabaoshan, Guangdong Province, China, were explored through various analytical methods, aiming to reveal the occurrence state and embedding characteristics of critical metal W in the ore. X-ray fluorescence analysis (XRF), powder X-ray diffraction (powder XRD), and scanning electron microscopy and energy dispersive spectroscopy (SEM−EDS) results show that the grade of critical metal W is 1.35%, and its main minerals are tungsten-bearing goethite and quartz. Micro-area XRD and mineral liberation analyzer (MLA) results indicate that ferrotungsten ore ($(W,Fe)(O,OH)_3$), the tungsten-bearing phase, was mainly present in the form of stripped and banded goethite. The valuable element distribution in major minerals was also quantitatively determined. Moreover, a possible mechanism for the evolution and formation of tungsten-bearing goethite weathering was discussed, and a combined flowsheet of beneficiation–metallurgical separation was proposed to provide a theoretical basis for the high-efficient recovery of critical metal W from tungsten-bearing goethite.

Key words: tungsten-bearing goethite; occurrence state; micro-area X-ray diffraction

1 Introduction

Tungsten has unique properties, such as the highest melting point of all non-alloyed metals [1−4], making it an essential component in various products across numerous fields, especially as a staple ingredient in high-speed steel tools [5]. This strategic and critical material is classified as such by US Department of Defense, European Commission, Government of the Russian Federation, UK Government, and Geoscience Australia [6]. However, only scheelite ($CaWO_4$) and wolframite ($(Fe,Mn)WO_4$) are economically significant tungsten-bearing minerals [7−9]. Despite the importance of tungsten, obtaining marketable tungsten concentrates with a satisfactory grade (60%−70% WO_3) is challenging.

Due to the challenge of achieving marketable tungsten concentrates with a satisfactory grade (60%−70% WO_3), many tungsten-bearing minerals, such as tungsten-bearing goethite [10], tungsten-bearing rutile [7], tungsten-bearing molybdenite [11], low-grade tungsten-bearing quartz vein [12], low-grade tungsten-bearing sheeted vein [13], low-grade tungsten-bearing granite [14], even low-grade calcic tungsten-bearing skarn [15], are still not economically viable for extraction in the industry.

Tungsten-bearing goethite is a promising source of tungsten due to its abundant reserves, high tungsten content, and presence of valuable elements, making it a strong contender as the third

Corresponding author: Yang CAO, E-mail: caoyang@csu.edu.cn
DOI: 10.1016/S1003-6326(24)66469-1

source of tungsten. These types of tungsten ores are widely distributed in Guangdong, Hunan, and Yunnan provinces of China, as well as in the Western Rhodopes of Bulgaria, typically with a tungsten content larger than 0.25%. However, most of them remain unused or are disposed of in tailings dams. For instance, more than 20 million tons of tungsten-bearing goethite have not been recovered for a long time at the Dabaoshan mine in Guangdong province, China. The primary reason is a lack of relevant process mineralogy and an efficient extraction method for the tungsten-bearing goethite, as existing methods for scheelite and wolframite, including density methods, magnetic separations, and flotation, have not yielded satisfactory results.

To ensure effective extraction of tungsten-bearing goethite, a thorough understanding of its chemical and process mineralogical characteristics is crucial. However, such studies are lacking in the existing literature. This study aimed to address this gap by applying various analytical techniques, including X-ray fluorescence (XRF), powder X-ray diffraction (XRD), and mineral liberation analyzer (MLA), to tungsten-bearing goethite samples. Additionally, scanning electron microscopy (SEM) and micro-area XRD were utilized to identify the main W occurrence and possible formation mechanism in the samples. Based on these analytical results, alternative enrichment and extraction methods were discussed, and a promising flowsheet for recovering critical metal W from tungsten-bearing goethite was proposed.

2 Experimental

2.1 Sampling and elemental analysis

The tungsten-bearing goethite sample used in this study was obtained from the Guangdong Dabaoshan mine in China, situated at the intersection of the northeast-trending Beijiang fault and the east-west trending Dadongshan−Guidong structural belt within the Shaoguan−Wuchuan deep fault. The mineralization of Fe, W, and Mo mainly occurred in the early Cretaceous period and large-scale deposits of iron−tungsten and molybdenum−tungsten were formed through a single process of tectonic−magmatic activity at different stages of magma differentiation and evolution. Exploration conducted in the 1950s and 1960s revealed that the Dabaoshan deposit held approximately 100 million tons of iron ore reserves, primarily of the weathering−leaching accumulation type.

Demineralized water was used throughout the experiments. Elemental analysis of the sample was performed using X-ray fluorescence (XRF) spectrometry (PANalytical Axios mAX, Netherlands) at the School of Minerals Processing and Bioengineering, Central South University, China.

2.2 Powder X-ray diffraction analysis

The mineralogical composition of the powder samples was determined using powder X-ray diffraction (PXRD) data, which were collected on a D8 Advance automatic diffractometer at the School of Geosciences and Info-physics, Central South University, China, in the Bragg−Brentano geometry. The samples were prepared using standard procedures before XRD analysis.

2.3 SEM−EDS analysis

The scanning electron microscopy−energy dispersive X-ray spectrometry (SEM−EDS) analysis was conducted using a FEI Quanta 650 environmental scanning electron microscope with a Bruker Quantax 200 dual silicon-drift energy dispersive X-ray spectrometer at the Changsha Research Institute of Mining and Metallurgy Co., Ltd., China Minmetals Corporation. To observe the cross-sectional morphology of the particles, the samples were mounted using Bakelite polymer and were ground and polished with 0.5 μm polishing paper. Each sample was carbon-coated for the SEM examination after polishing and cleaning.

2.4 Micro-area XRD analysis

The micro-area XRD analysis was performed using D/max rapid IIR diffractometer (Rigaku Corporation, Tokyo, Japan) at the School of Geosciences and Info-physics, Central South University, China. A Cu target tube and graphite monochromator at 40 kV and 100 mA were utilized [16].

2.5 Mineral liberation analysis

Quantitative mineralogy study was conducted using a FEI MLA 650 system at the Changsha Research Institute of Mining and Metallurgy Co.,

Ltd., China Minmetals Corporation. This automated scanning electron microscopy (SEM) system, known as the mineral liberation analyzer (MLA), identifies and quantifies minerals based on their backscattered electron (BSE) level and compares the collected spectrum shape to a mineral database [17,18]. The system comprises a Quanta 650 environmental SEM and a Bruker Quantax 200 dual silicon-drift energy dispersive X-ray spectrometer [19].

3 Results and discussion

3.1 Sampling and elemental analysis results

The X-ray fluorescence (XRF) analysis (Table 1) of the tungsten-bearing goethite sample revealed the W content of 1.35%, which is significantly higher than that of typical scheelite [20] and wolframite [21] ores. The sample also contains Mn, Al, and Si at concentrations of 3.28%, 2.33%, and 8.14%, respectively. Additionally, the presence of small amounts of 0.04% Cu, 0.21% Pb, 0.08% Zn, and 0.15% S suggests the existence of sulfide ores, while trace amounts of Ca, K, Mo, and Bi were also detected.

Table 1 Element contents in tungsten-bearing goethite (wt.%)

W	Fe	Mn	Mo	Cu	Pb	Zn	Bi	Ba
1.35	44.91	3.28	0.084	0.04	0.21	0.08	0.16	0.08
Na	Mg	Al	K	Ca	O	Si	S	P
0.03	0.07	2.33	0.1	0.84	37.68	8.14	0.15	0.08

Powder X-ray diffraction (Fig. 1) was used to analyze the phase composition of the tungsten-bearing goethite ore. The analysis showed that the major iron-bearing phase present was goethite (FeOOH), while the major silicon-bearing phase was quartz (SiO_2). Additionally, minor phases of andradite ($Ca_3Fe_{1.88}(SiO_4)_3$) and ramsdellite (MnO_2) were identified. However, due to the low W content and poor crystallinity of the sample, it was difficult to accurately distinguish the tungsten-bearing phases.

3.2 Occurrence state of tungsten in tungsten-bearing minerals

3.2.1 Tungsten-bearing goethite

Goethite is the dominant tungsten-bearing species and primary phase in the ore. The EDS analysis in Fig. 2 reveals four different types of tungsten-bearing goethite, as presented in Table 2.

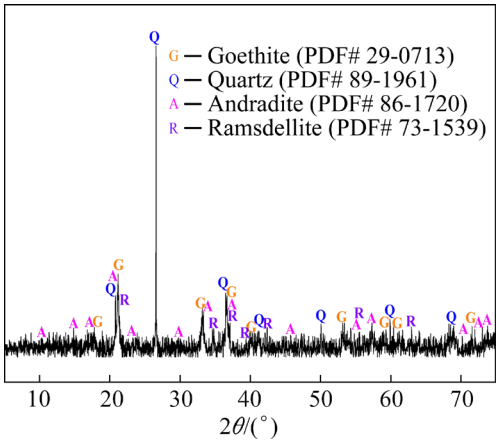

Fig. 1 Powder X-ray diffraction pattern of tungsten-bearing goethite

The primary differences among these types of tungsten-bearing goethites lie in the content and distribution of tungsten. In Fig. 2(a), Areas 1 and 3 illustrate tungsten with a banding distribution among the goethite particles. The W contents are 20.90% and 26.51%, while the Fe contents are approximately 45%. On the other hand, other types of tungsten-bearing goethite exhibit a uniform distribution, with W contents ranging from 3% to 30%. For instance, Fig. 2(b) displays a typical goethite with high W content in Area 6, containing 22.12% W and 47.27% Fe. Furthermore, Fig. 2(d) depicts a typical goethite with low W content, containing only 3.69% W but 60.12% Fe in Area 13. Additionally, the third type of tungsten-bearing goethite presents equidistributional tungsten and molybdenum, as illustrated in Fig. 2(c). Taking Area 5 as an example, it contains 8.72% W, 0.054% Mo, and 53.01% Fe. Some goethite particles have more than 60% Fe but no detectable W or Mo, as shown in Areas 2 and 4.

To clarify the distribution of stripped and banded forms of tungsten-bearing goethite particles, an EDS analysis was conducted. Figure 3 reveals that the W element is uniformly distributed within the tungsten-bearing goethite phase. The corresponding EDS line scan across the particle demonstrates the presence of stripped and banded regions with high W content located close to gaps and cracks in the goethite phase, as seen in the light grey region. Conversely, the dark grey region

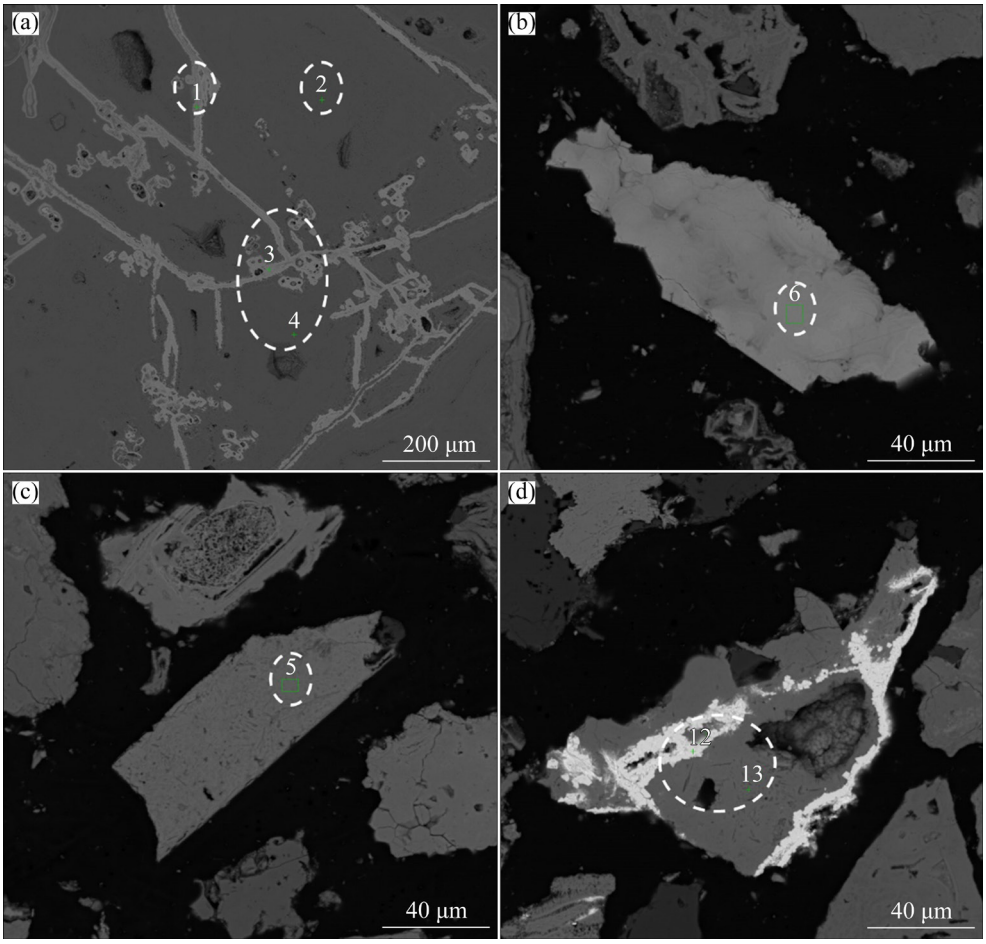

Fig. 2 SEM images of different tungsten-bearing goethite particles

Table 2 Element contents in tungsten-bearing goethite particles (wt.%)

Area No. in Fig. 2	W	Bi	Mo	Fe	Mn	O	Si	Al
1	20.9			46.98	0.34	31.56	0	0.2
2				61.83	0.42	35.92	1.27	0.4
3	26.51			44.42	0.3	28.53		0.18
4				63.77	0.4	35.01	0.81	
5	8.72		0.054	53.01	0.35	34.65	0.47	2.49
6	22.12			47.27	0.37	29.74		0.36
12	36.89	32.97		13.72		16.3		
13	3.69			60.12	0.39	33.92	0.52	1.22

represents the normal goethite phase, which has lower W content and higher Fe content. Overall, the EDS line scan profile of the W element confirms that the tungsten-bearing phase is distributed among the goethite in both stripped and banded forms.

These observations have the important implications, as they suggest that the formation of tungsten-bearing goethite may be attributed to weathering and erosion processes. These processes could be responsible for the banded distribution of tungsten and the large range of W content found in other homogeneous tungsten-bearing goethite. It is also worth noting that conventional physical separation methods may not be effective in enriching W in equidistributional tungsten-bearing goethite, as fine grinding is required to separate the

banded distribution of tungsten-bearing goethite. However, this process may have low separation efficiency due to the high Fe content.

3.2.2 Tungsten-bearing psilomelane

Figure 4 displays the two kinds of tungsten-bearing psilomelane, a typical mineral with low W content [22], which were found in the samples. Table 3 presents the results of elemental composition analysis of the particles using EDS. The first type of tungsten-bearing psilomelane (Area 7 in Fig. 4(a)) contains 0.79% W, 2.79% Ba, 2.26% Al, and 61.17% Mn. The second type, depicted in Fig. 4(b), contains not only Pb and Fe but also W and Mn. For instance, Area 20 of this type contains 0.69% W, 12.83% Pb, 10.67% Fe, and 42.37% Mn.

3.2.3 Other tungsten-bearing minerals

The sample contains small quantities of some commonly occurring independent tungsten minerals, but these minerals have a high W content, as demonstrated in Table 4. Figure 5(a) illustrates a

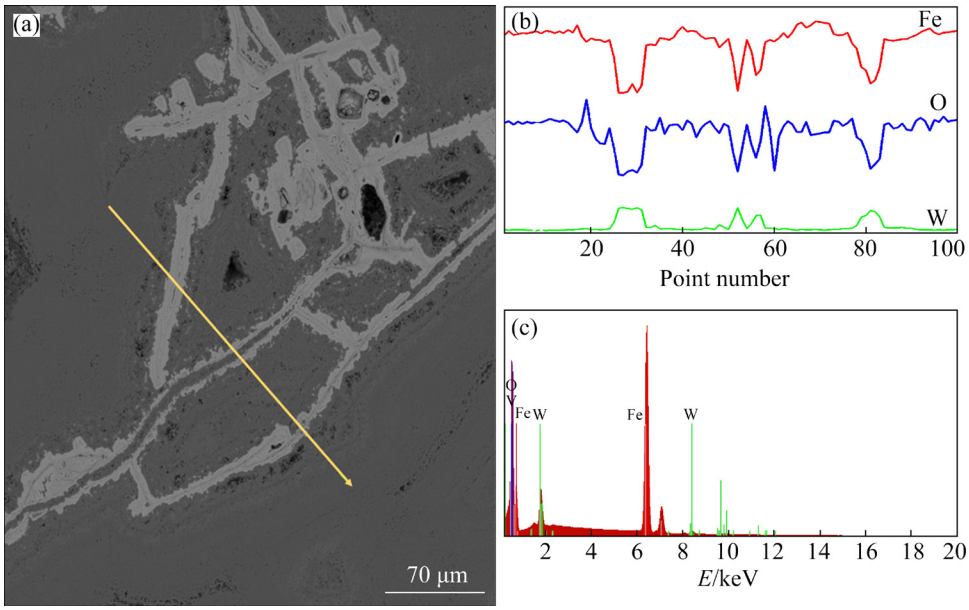

Fig. 3 SEM−EDS line scans of tungsten-bearing goethite particles: (a) SEM image; (b) EDS plot along line scan; (c) Average EDS spectrum of line scan

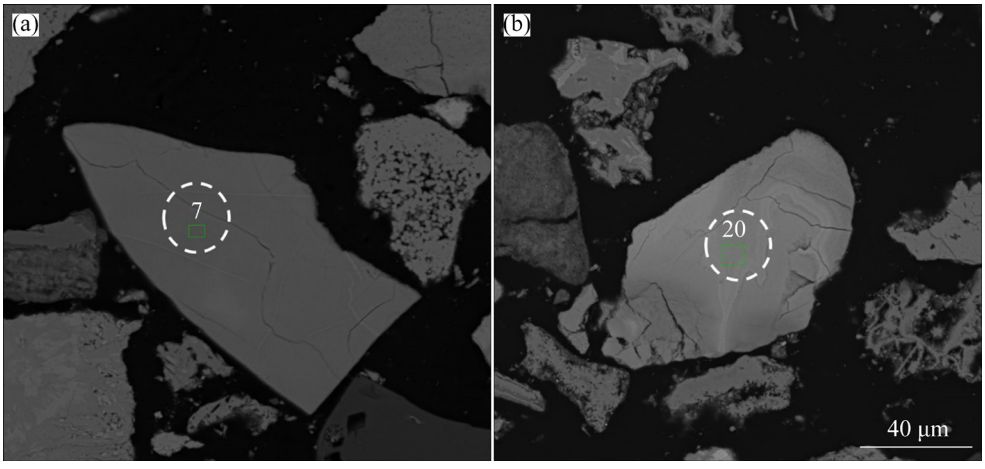

Fig. 4 SEM images of tungsten-bearing psilomelane particles

Table 3 Element contents in tungsten-bearing psilomelane particles (wt.%)

Area No. in Fig. 4	W	Ba	Pb	Fe	Mn	O	Al	K	Ca
7	0.79	2.79			61.17	32.05	2.26	0.63	0.3
20	0.69	0.04	12.83	10.67	42.37	31.48	1.39	0.32	0.01

Table 4 Element contents in other tungsten-bearing mineral particles (wt.%)

Area No. in Fig. 5	W	Bi	Pb	Ca	S	Fe	Mn	Si	O
11	60.89					19.67	0.21		19.22
14	55.05	18.54				9.59	0.56		16.25
15	57.17		11.72			10.35			20.76
16	2.68			0.07		59.25	0.22	0.09	36.75
17	61.7			15.35		2.25			20.7
18					51.1	48.9			
19						0.78		50.17	48.6

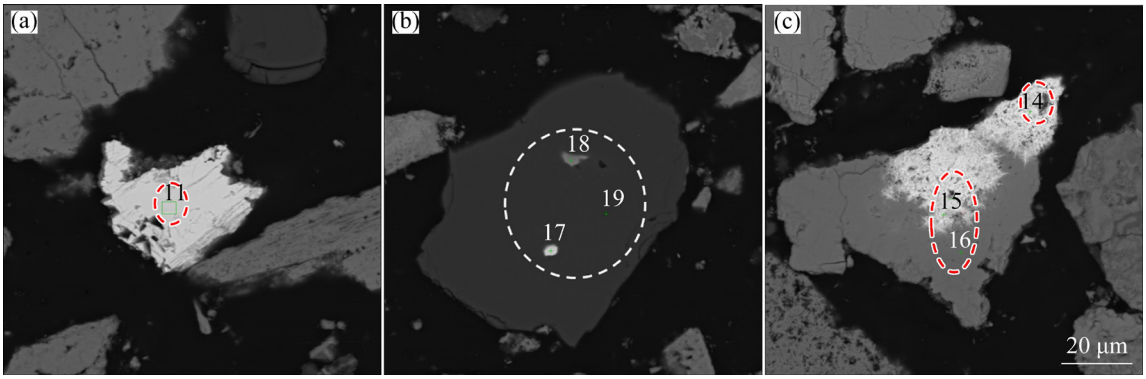

Fig. 5 SEM images of other tungsten-bearing mineral particles

wolframite [23] ((Fe,Mn)WO_4) particle with W and Fe contents of 60.89% and 19.67% (Area 11), respectively. Figure 5(b) shows a scheelite ($CaWO_4$) particle (Area 17) embedded in a quartz particle with a pyrite particle that has W and Ca contents of 61.70% and 15.35%, respectively. Figure 5(c) depicts stolzite [24] ($PbWO_4$, Area 15) and russellite [25] (Bi_2WO_6, Area 14) particles associated with goethite, which has low W content. Stolzite and russellite particles exhibit anomalous and rough morphology, being porous and possessing needle-like edges. These results suggest that these minerals are likely secondary minerals with low crystallinity.

3.2.4 Molybdenum-bearing goethite

The tungsten-bearing goethite ore also contains valuable amounts of Mo, which exists in two forms of molybdenum-bearing goethite (Fig. 6). The composition of these particles was analyzed using EDS, and the results are presented in Table 5. Figure 6(a) displays the first type of molybdenum-bearing goethite, which has a content of 0.609% of Mo, 0.47% of Mn, 0.82% of Al, and 61.09% of Fe (Area 8). Figure 6(b) shows the other type of molybdenum-bearing goethite, which contains both Mo and W. As a example, Area 9 has 0.321% of

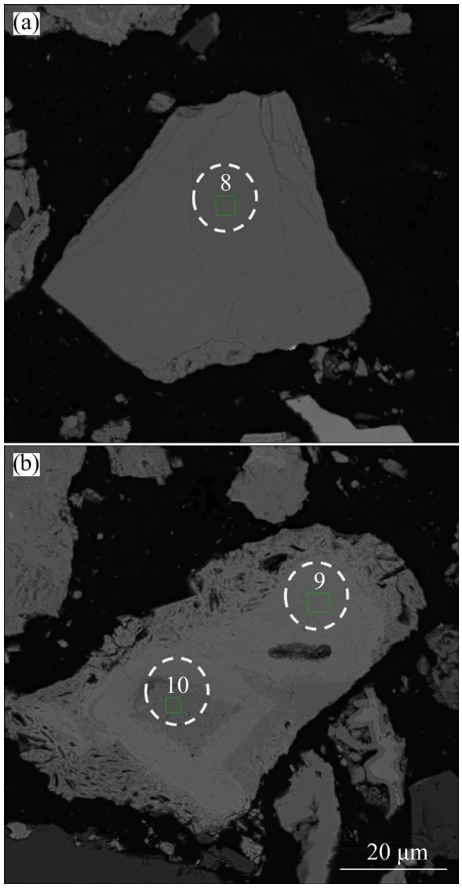

Fig. 6 SEM images of molybdenum-bearing goethite particles

Table 5 Element contents in molybdenum-bearing goethite particles (wt.%)

Area No. in Fig. 6	W	Mo	Fe	Mn	O	Al	Si
8		0.609	61.09	0.47	36.47	0.82	0.38
9	3.42	0.312	63.46	0.41	31.08	0.88	0.40
10			64.63	0.39	34.11	0.08	0.78

Mo, 3.42% of W, 0.41% of Mn, and 63.46% of Fe. Additionally, a goethite particle (Area 10) is embedded in this type of molybdenum-bearing goethite. The edges of this particle exhibit a porous and multilayer structure, which is similar to the result of the weathering and erosion.

3.3 Tungsten-bearing goethite phase identification

Tungsten-bearing goethite is the primary tungsten-bearing particle, but its phase remains unclear. Micro-area XRD was utilized to identify the main W phase. By considering the analyzed spot size diameter is approximately 100 μm [26], it is preferable to perform the analysis on a single tungsten-bearing goethite particle. Therefore, an unground crushed ore sample was mounted using the Bakelite polymer and polished with polishing paper. After polishing and cleaning, the mounted sample (Fig. 7) was observed by SEM to locate tungsten-bearing goethite particles. Three particles (Points 1, 2, and 3 in Figs. 7(a, b)) were selected and marked (by the yellow circles in Fig. 7) for micro-area XRD analysis, which had a relatively larger tungsten-bearing goethite detecting area (by the red rectangle in Figs. 7(a, b)). Finally, the sample was transferred to an object stage for micro-area XRD.

The micro-area XRD analysis inferred that the tungsten-bearing phase is ferritungstite ($(W,Fe)(O,OH)_3$) (Fig. 8) in three points in Fig. 7,

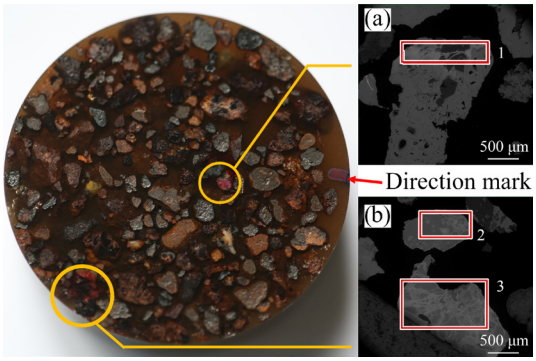

Fig. 7 Sample preparation for micro-area XRD

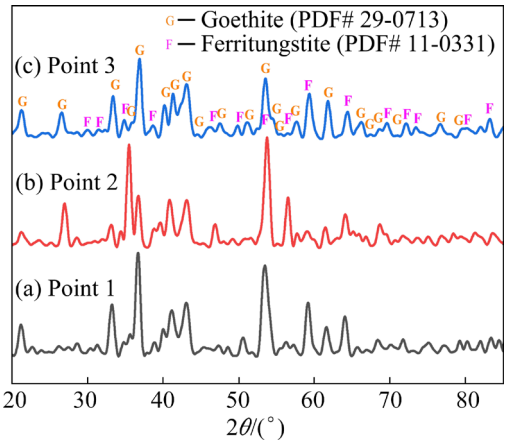

Fig. 8 Micro-area XRD patterns of tungsten-bearing phase

along with the presence of goethite phase. The similarities in physical properties and structure between ferritungstite and goethite suggest that it would be challenging to separate them through physical beneficiation techniques such as gravity, flotation, and magnetic or electrostatic separation [27]. Moreover, the high Fe content of the samples makes it difficult to effectively remove Fe ions using hydrometallurgical methods involving acid or alkali leaching.

3.4 Main mineral and elements distribution

Mineral liberation analysis (MLA) can efficiently acquire robust classification and mineralogical data [28], and can provide detailed information on the composition of single particles and particle populations exposed on the cross-sectioned surface of a grain mount [29]. Mineral composition and contents in the tungsten-bearing goethite ore are presented in Table 6. The sample contains approximately 80% goethite, which can be categorized into three types: pure goethite, accounting for only 0.81%, goethite (Mn,Al), which contains Mn and Al and accounts for 21.29%, and tungsten-bearing goethite (goethite (W)), the highest content mineral, containing W, Mo, Mn, and Al and accounting for 57.49%. Additionally, independent tungsten-bearing minerals, such as stolzite, wolframite, russellite, and scheelite, account for only 0.12%. Other manganese-bearing minerals, including psilomelane and pyrolusite, account for 3.81% and 0.77%, respectively. The major gangue minerals, quartz, andradite, and muscovite, account for 9.14%, 3.77%, and 1.48%,

Table 6 Main minerals in tungsten-bearing goethite ore (wt.%)

Mineral	Content	Mineral	Content	Mineral	Content
Goethite (W)	57.49	Corundum	0.07	Diopside	0.0059
Goethite (Mn,Al)	21.29	Calcite	0.043	Albite	0.005
Goethite	0.81	Chlorite	0.034	Orthoclase	0.0043
Quartz	9.15	Bismite	0.029	Fluorite	0.0043
Psilomelane	3.81	Pyrite	0.019	Talc	0.0038
Andradite	3.77	Wolframite	0.019	Scheelite	0.0033
Muscovite	1.48	Russellite	0.019	Cassiterite	0.0022
Kaolinite	0.79	Apatite	0.011	Phlogopite	0.0015
Pyrolusite	0.77	Rutile	0.009	Titanite	0.0012
Serpentine	0.13	Pyrrhotite	0.0081	Molybdenite	0.0004
Magnetite	0.11	Sphalerite	0.0074	Others	0
Stolzite	0.076	Chalcopyrite	0.007	Total	100

respectively. These aforementioned minerals constitute almost 98% of the total mineral content.

MLA can also be used to determine the distribution of valuable elements in major minerals, which helps to identify the most valuable minerals, design separation procedures, and understand the distribution features of desired elements [30]. Figure 9 displays the element distribution of the main minerals detected by MLA, demonstrating that tungsten-bearing goethite (goethite (W)) contains 91.61% of W and 99.60% of Mo. Psilomelane and stolzite contain 4.82% and 2.27% of W, respectively, whereas only 1.30% of W is present in the form of wolframite, russellite, and scheelite. Besides, tungsten-bearing goethite contains 17.56% of Mn and 21.93% of Al, while Mn/Al-bearing goethite (goethite (Mn,Al)) contains 7.04% of Mn and 46.15% of Al. Moreover,

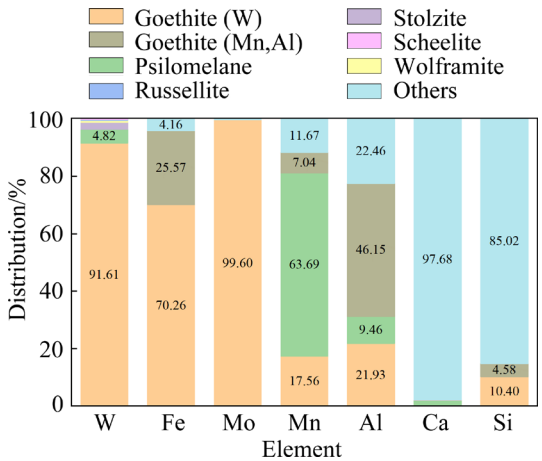

Fig. 9 Elements distribution in main phases

psilomelane contains 63.69% Mn and 9.46% Al. These results suggest that tungsten-bearing goethite is the primary tungsten and molybdenum-bearing mineral to be recovered, and it can be easily separated from silicate minerals like quartz and muscovite. However, it cannot be effectively separated from other goethite, psilomelane, and andradite since they have similar density, magnetism, and flotation properties.

3.5 Possible formation mechanism of tungsten-bearing goethite

The weathering process is considered the main formation mechanism of this tungsten-bearing goethite ore. It has been reported that significant amounts of W can be incorporated into the crystal structures of hematite (α-Fe_2O_3) and goethite (α-FeOOH) through a heterovalent substitution mechanism, where one W atom replaces three Fe atoms [31]. Based on this information, a detailed possible formation mechanism of the tungsten-bearing goethite can be described in the following steps:

(1) Weathering and hydrolysis of sulfide ore

Pyrite and marcasite are common minerals in mine environments that cause acid generation since they may generate acidic drainage upon exposure to atmospheric conditions [32]. Besides, Fe sulfates are common weathering products of Fe sulfide oxidation in mining environments, and Fe(III) resulting from Fe sulfate mineral dissolution can undergo hydrolysis, resulting in the release of H^+

(Eqs. (1) and (2)):

$$4FeS_2+15O_2+2H_2O=2Fe_2(SO_4)_3+2H_2SO_4 \quad (1)$$

$$Fe_2(SO_4)_3+6H_2O=2Fe(OH)_3+3H_2SO_4 \quad (2)$$

(2) Weathering and destruction of primary W minerals

For example, the scheelite is most probably dissolved at pH<6 with the formation of polytungstate ions [33]. These ion forms of W are capable of long-distance transport in solution:

$$MWO_4+2H^+=M^{2+}+H_2WO_4 \text{ (M: Ca, Mn, Fe)} \quad (3)$$

(3) Formation of secondary tungsten minerals

As the weathering proceeds, part of W and Fe are transited from the minerals into the supergene solution. Meanwhile, the amount of sulfide ore decreases, and the solution gradually changes from acidic to slightly alkaline. Then, the hydrolysis products of Fe(III) react with polytungstate ions in the weak acidic or alkaline medium (pH>3), which crystallizes in situ at the expense of meymacite and forms secondary tungsten minerals involving ferritungstite:

$$Fe(OH)_3+H_2WO_4=(W,Fe)(O,OH)_3+H_2O \quad (4)$$

These processes are carried out in situ and ex situ, involving the ground waters and essential transport of dissolved W, including its polytungstate ion forms [10]. Once the W is incorporated, it would immobilize for as long as these phases are stable, potentially economic W resources. Besides, molybdenite may weather secondary minerals such as ferrimolybdite via similar steps.

3.6 Flowsheet for comprehensive recovery of tungsten-bearing goethite

The special properties and formation process of tungsten-bearing goethite make it unsuitable for conventional flotation and gravity concentration method [10]. Detailed research results can provide fundamental theoretical data to improve the beneficiation process flow and the processing index of tungsten-bearing goethite ore, recycle other valuable minerals, and comprehensively utilize tailings [34]. Based on the chemical and process mineralogical characterizations of tungsten-bearing goethite, a new flowsheet for the comprehensive recovery of tungsten-bearing goethite is proposed, as illustrated in Fig. 10.

As shown in Fig. 10, the ores are crushed and ground to suitable sizes, followed by magnetic or gravity separation, which can be used to separate the magnetic or high-density mineral from non-magnetic or light gangue minerals such as quartz. The primarily concentrate is then treated by desulfurization flotation to separate sulfide minerals, including Fe, Cu, Pb, and Zn sulfide [35] from oxide minerals such as tungsten and molybdenum-bearing goethite, which could help to not only recover some nonferrous metals mineral resources but also reduce the sulfur dioxide emissions in the subsequent processing. The W, Mo, and Fe content is slightly enriched in the flotation tailings but could not be efficiently recovered by conventional beneficiation. Therefore, pyrometallurgy and hydrometallurgy are suggested to further extract W, Mo, Fe, and Mn, respectively. The proposed flow-sheet, which combines beneficiation−metallurgy to treat the tungsten-bearing goethite, is a promising comprehensive recovery method for this tungsten ore.

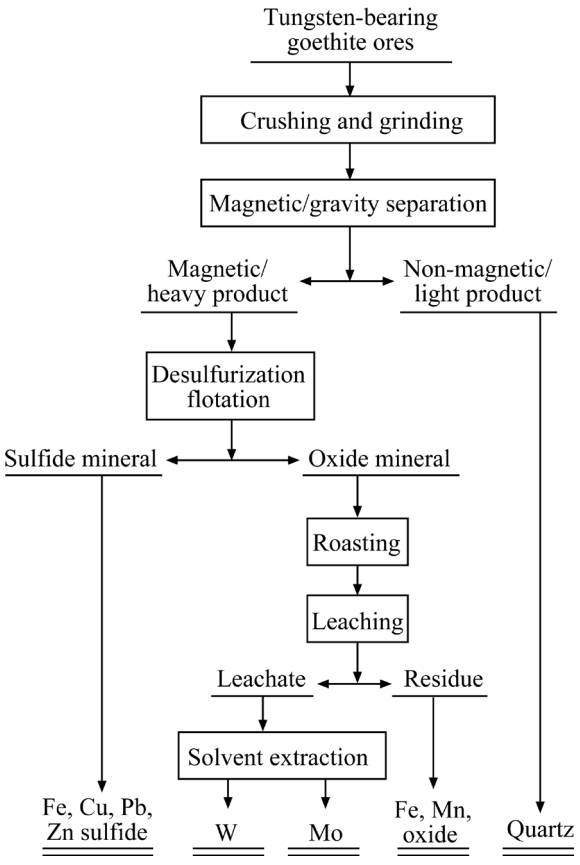

Fig. 10 Flowsheet for comprehensive recovery of tungsten-bearing goethite

4 Conclusions

(1) The XRF, powder X-ray diffraction, and

SEM−EDS results show that the contents of the main valuable elements W, Fe, Mn, Al, and Si in this ore are 1.35%, 44.91%, 3.28%, 2.33%, and 8.14%, respectively. Its main minerals are tungsten-bearing goethite, quartz, and some sulfide ore. Besides, four types of tungsten-bearing goethite, tungsten-bearing psilomelane, and molybdenum-bearing goethite were observed.

(2) The micro-area XRD and MLA analyses indicate that the tungsten-bearing phase is ferritungstite ($(W,Fe)(O,OH)_3$) and distributes among the goethite in stripped and banded forms, which cannot be effectively upgraded by traditional physical beneficiation processes. It is also confirmed that approximately 80% of the sample consists of goethite, and 57.49% is tungsten-bearing goethite. Meanwhile, the distribution of valuable elements in major minerals is also quantitatively determined, showing that 91.61% of W and 99.60% of Mo exist in the tungsten-bearing goethite.

(3) The formation mechanism of tungsten-bearing goethite can be described in detail by the following three steps: First, the sulfide ore undergoes weathering and hydrolysis; Second, primary tungsten-bearing minerals undergo weathering and destruction; Third, secondary tungsten-bearing minerals are formed.

(4) Based on these chemical and process mineralogical characterizations, a combined flowsheet of beneficiation−metallurgy to treat the tungsten-bearing goethite is proposed, which can efficiently separate valuable from barren particles and it is a promising comprehensive recovery method for this kind of tungsten ores.

CRediT authorship contribution statement

Hong-hu TANG and **Bing-jian LIU:** Investigation, Formal analysis, and Writing − Original draft; **Cui WANG** and **Xiong-xing ZHANG:** Formal analysis, Data curation, Investigation, Writing − Review and editing; **Hai-sheng HAN**, **Li WANG,** and **Yang CAO:** Methodology, Supervision, Writing − Review and editing; **Wei SUN:** Project administration, Conceptualization, Resources, Methodology, and Funding acquisition.

Declaration of competing interest

The authors declare that they have no known competing financial interests or personal relationships that could have appeared to influence the work reported in this paper.

Acknowledgments

We gratefully appreciate the financial support from the National Key R&D Program of China (No. 2022YFC2904501), the National Natural Science Foundation of China (Nos. 52004335, 91962223), the Natural Science Foundation of Hunan Province, China (No. 2023JJ20071), and Hunan International Joint Research Center for Efficient and Clean Utilization of Critical Metal Mineral Resources, China (No. 2021CB1002).

References

[1] WANG Xu, QING Wen-qing, DONG Liu-yang, GUO Jian-gen, ZHANG Jian, YANG Cong-ren. Review of tungsten resource reserves, tungsten concentrate production and tungsten beneficiation technology in China [J]. Transactions of Nonferrous Metals Society of China, 2022, 32: 2318−2338.

[2] LÜ Ze-peng, JIAN Kai-liang, DANG Jie. Effect of salt-assisted reduction method on morphologies and size of metallic tungsten particles [J]. Transactions of Nonferrous Metals Society of China, 2020, 30: 3133−3146.

[3] WANG Kai-fei, ZHANG Guo-hua. Synthesis of high-purity ultrafine tungsten and tungsten carbide powders [J]. Transactions of Nonferrous Metals Society of China, 2020, 30: 1697−1706.

[4] SHI Xin-wei, ZHANG Sen, ZHOU Qiang, LI Jing, ZHU Bai-lin, XU Liu-jie, GAO Qi-long. Effect of surface modification on thermal expansion of $Zr_2WP_2O_{12}$/aromatic polyimides based composites [J]. Tungsten, 2023, 5: 179–188.

[5] LI Shu-cong, WANG Qing-lin, YAO Yu, SANG Dan-dan, ZHANG, Hai-wa, ZHANG Guo-zhao, WANG Cong, LIU Cai-long. Application of high-pressure technology in exploring mechanical properties of high-entropy alloys [J]. Tungsten, 2023, 5: 50–66.

[6] CHAKHMOURADIAN A R, SMITH M P, JYNICKY J. From “strategic” tungsten to “green” neodymium: A century of critical metals at a glance [J]. Ore Geology Reviews, 2015, 64: 455−458.

[7] YANG Xiao-sheng. Beneficiation studies of tungsten ores—A review [J]. Minerals Engineering, 2018, 125: 111−119.

[8] CHEN Shu-jun, ZHAO Hua-jun, CHEN Si-yi, WEN Pu-shan, WANG Hao, LI Wen-po. Camphor leaves extract as a neoteric and environmentally friendly inhibitor for Q235 steel in HCl medium: Combining experimental and theoretical researches [J]. Journal of Molecular Liquids, 2020, 312: 113433.

[9] CHEN Yuan-lin, GUO Xue-yi, WANG Qin-meng, TIAN Qing-hua, ZHANG Jin-xiang, HUANG Shao-bo. Physicochemical and environmental characteristics of alkali leaching residue of wolframite and process for valuable metals recovery [J]. Transactions of Nonferrous Metals Society of China, 2022, 32: 1638−1649.

[10] TARASSOV M, TARASSOVA E. Modes of occurrence of tungsten in oxidized ores of the Grantcharitsa tungsten deposit (Western Rhodopes, Bulgaria) [C]//17th Serbian Geological Congress. Serbia, 2019: 82−85.

[11] SILVA D P T, FIGUREUEIREDO O M, VEIGA J P, BATISTA M J, NORONHA F. Tungsten-bearing molybdenite from borralha [C]//X Congresso Ibérico de Geoquímica/XVIII Semana de Geoquímica. Alfragide, 2015: 151−154.

[12] FRANCIS C A, DYAR M D, WILLIAMS M, HUGHES J M, The occurrence and crystal structure of foitite from a Tungsten-bearing vein at Copper Mountain, Taos County, New Mexico [J]. The Canadian Mineralogist, 1999, 37(6): 1431−1438.

[13] SANDERSON D J, ROBERTS S, GUMIEL P, GREENFIELD C. Quantitative analysis of tin- and tungsten-bearing sheeted vein systems [J]. Economic Geology, 2008, 103(5): 1043−1056.

[14] ZHANG Yang, YANG Jin-hui, CHEN Jing-yuan, WANG Hao, XIANG Yuan-xin. Petrogenesis of Jurassic tungsten-bearing granites in the Nanling Range, South China: Evidence from whole-rock geochemistry and zircon U–Pb and Hf–O isotopes [J]. Lithos, 2017, 278/279/280/281: 166−180.

[15] TORNOS F, GALINDO C, CRESPO J L, SPIRO B F. Geochemistry and origin of calcic tungsten-bearing skarns, Los Santos, Central Iberian Zone, Spain [J]. The Canadian Mineralogist, 2008, 46(1): 87−109.

[16] XIE Xian-de, CHEN Ming. Suizhou Meteorite: Mineralogy and Shock Metamorphism [M]. 2nd ed. Guangzhou: Guangdong Science and Technology Press, 2015.

[17] FANDRICH R, GU Ying, BURROWS D, MOELLER K. Modern SEM-based mineral liberation analysis [J]. International Journal of Mineral Processing, 2007, 84: 310−320.

[18] CELEP O, SERBEST V. Characterization of an iron oxy/hydroxide (gossan type) bearing refractory gold and silver ore by diagnostic leaching [J]. Transactions of Nonferrous Metals Society of China, 2015, 25: 1286−1297.

[19] LAAKSO K, MIDDLETON M, HEINIG T, BARS R, LINTINEN P. Assessing the ability to combine hyperspectral imaging (HSI) data with Mineral Liberation Analyzer (MLA) data to characterize phosphate rocks [J]. International Journal of Applied Earth Observation and Geoinformation, 2018, 69: 1−12.

[20] HAN Hai-sheng, XIAO Yao, HU Yue-hua, SUN Wei, NGUYEN A V, TANG Hong-hu, GUI Xia-hu, XING Yao-wen, WEI Zhao, WANG Jian-jun. Replacing Petrov's process with atmospheric flotation using Pb-BHA complexes for separating scheelite from fluorite [J]. Mineral Engineering, 2020, 145: 106053.

[21] AI Guang-hua, YANG Xiu-li, LI Xiao-bo. Flotation characteristics and flotation kinetics of fine wolframite [J]. Powder Technol, 2017, 305: 377−381.

[22] SOBOLEV R N, PELYMSKIY G A. Evolutionary history of tungsten metallization [J]. Journal of Southeast Asian Earth Sciences, 1993, 8: 387−390.

[23] LIU Xiang-chong, XIAO Chang-hao. Wolframite solubility and precipitation in hydrothermal fluids: Insight from thermodynamic modeling [J]. Ore Geology Reviews, 2020, 117: 103289.

[24] PERKINS C K, REED T M, BROWN Z A, APBLETT A W. Exceptional sorption behaviour of porous tungsten oxide for aqueous lead [J]. Environmental Science: Water Research & Technology, 2017, 3: 429−432.

[25] OKUDERA H, SAKAI Y, YAMAGATA K, TAKEDA H. Structure of russellite (Bi_2WO_6): Origin of ferroelectricity and the effect of the stereoactive lone electron pair on the structure [J]. Acta Crystallographica Section B−Structural Science Crystal Engineering and Materials, 2018, 74: 295−303.

[26] QIN Wen, FU Li-cai, ZHU Jia-jun, YANG Wu-lin, LI De-yi, ZHOU Ling-ping. Tribological properties of self-lubricating Ta-Cu films [J]. Applied Surface Science. 2018, 435: 1105−1113.

[27] TANG Hong-hu, SUN Wei, HU Yue-hua, HAN Hai-sheng. Comprehensive recovery of the components of ferritungstite base on reductive roasting with mixed sodium salts, water leaching and magnetic separation [J]. Mineral Engineering, 2016, 86: 34−42.

[28] SCHULZ B, MERKER G, GUTZMER J. Automated SEM mineral liberation analysis (MLA) with generically labelled EDX spectra in the mineral processing of rare earth element ores [J]. Minerals, 2019, 9: 527.

[29] LEIßNER T, BACHMANN K, GUTZMER J, PEUKER U A. MLA-based partition curves for magnetic separation [J]. Mineral Engineering, 2016, 94: 94−103.

[30] CELEP O, YAZICI E Y, ALTINKAYA P, DEVECI H. Characterization of a refractory arsenical silver ore by mineral liberation analysis (MLA) and diagnostic leaching [J]. Hydrometallurgy, 2019, 189: 105106.

[31] KREISSL S, BOLANZ R, GÖTTLICHER J, STEININGER R, TARASSOV M, MARKL G. Structural incorporation of W^{6+} into hematite and goethite: A combined study of natural and synthetic iron oxides developed from precursor ferrihydrite and the preservation of ancient fluid compositions in hematite [J]. American Mineralogist, 2016, 101: 2701−2715.

[32] JENNINGS S R, DOLLHOPF D J, INSKEEP W P. Acid production from sulfide minerals using hydrogen peroxide weathering [J]. Applied Geochemistry. 2000, 15: 235−243.

[33] KOUTSOSPYROS A, BRAIDA W, CHRISTODOULATOS C, DERMATAS D, STRIGUL N. A review of tungsten: From environmental obscurity to scrutiny [J]. Journal of Hazardous Materials, 2006, 136: 1−19.

[34] XU Cai-li, ZHONG Cheng-bin, LYU Ren-liang, RUAN Yao-yang, ZHANG Zhen-yue, CHI Ru-an. Process mineralogy of Weishan rare earth ore by MLA [J]. Journal of Rare Earths, 2019, 37: 334−338.

[35] MOHAMMADNEJAD S, NOAPARAST M, HOSSEINI S, AGHAZADEH S, MOUSAVINEZHAD S, HOSSEINI F. Physical methods and flotation practice in the beneficiation of a low grade tungsten-bearing scheelite ore [J]. Russian Journal of Nonferrous Metals, 2018, 59: 6−15.

大宝山含钨褐铁矿中钨的赋存状态与嵌布特征

唐鸿鹄[1,2]，刘丙建[1,2]，王 翠[1,2]，张雄星[1,2]，韩海生[1,2]，王 丽[1,2]，曹 杨[1,2]，孙 伟[1,2]

1. 中南大学 资源加工与生物工程学院，长沙 410083；
2. 中南大学 湖南省关键金属矿产资源高效清洁利用国际联合研究中心，长沙 410083

摘 要：通过多种分析方法，探究广东大宝山含钨褐铁矿的物相组成、元素分布等工艺矿物学特征，以揭示矿石中关键金属钨的赋存状态与嵌布特征。X 射线荧光分析(XRF)、粉末 X 射线衍射(XRD)以及扫描电子显微镜和能谱(SEM−EDS)结果表明：矿石中主要矿物为含钨褐铁矿和石英，关键金属钨品位为 1.35%。微区 X 射线衍射(Micro-XRD)和矿物解离度分析仪(MLA)结果表明：钨主要赋存于高铁钨华($(W,Fe)(O,OH)_3$)中，而高铁钨华则以剥离和带状形式紧密分布在褐铁矿中。同时，还定量分析了有价元素在各主要矿物中的赋存和分布情况，并讨论了含钨褐铁矿风化演变和形成机制。最终提出了一种选冶联合分选回收流程，为高效回收含钨褐铁矿中关键金属钨提供理论基础。

关键词：含钨褐铁矿；赋存状态；微区 X 射线衍射

(Edited by Bing YANG)